Gating of mammalian cardiac gap junction channels by transjunctional voltage

Hong-Zhan Wang,* Jian Li,‡ Larry F. Lemanski,‡ and Richard D. Veenstra*
Departments of *Pharmacology and ‡Anatomy and Cell Biology, State University of New York Health Science Center, Syracuse, New York 13210

ABSTRACT Numerous two-cell voltage-clamp studies have concluded that the electrical conductance of mammalian cardiac gap junctions is not modulated by the transjunctional voltage (V_j) profile, although gap junction channels between low conductance pairs of neonatal rat ventricular myocytes are reported to exhibit V_j-dependent behavior. In this study, the dependence of macroscopic gap junctional conductance (g_j) on transjunctional voltage was quantitatively examined in paired 3-d neonatal hamster ventricular myocytes using the double whole-cell patch-clamp technique. Immunolocalization with a site-specific antiserum directed against amino acids 252–271 of rat connexin43, a 43-kD gap junction protein as predicted from its cDNA sequence, specifically stained zones of contact between cultured myocytes. Instantaneous current–voltage (I_j–V_j) relationships of neonatal hamster myocyte pairs were linear over the entire voltage range examined ($0 \leq V_j \leq \pm 100$ mV). However, the steady-state I_j–V_j relationship was nonlinear for $V_j > \pm 50$ mV. Both inactivation and recovery processes followed single exponential time courses ($\tau_{inactivation}$ = 100–1,000 ms, $\tau_{recovery} \cong 300$ ms). However, I_j recovered rapidly upon polarity reversal. The normalized steady-state junctional conductance-voltage relationship (G_{ss}–V_j) was a bell-shaped curve that could be adequately described by a two-state Boltzmann equation with a minimum G_j of 0.32–0.34, a half-inactivation voltage of −69 and +61 mV, and an effective valence of 2.4–2.8. Recordings of gap junction channel currents (i_j) yielded linear i_j–V_j relationships with slope conductances of ~20–30 and 45–50 pS. A kinetic model, based on the Boltzmann relationship and the polarity reversal data, suggests that the opening (α) and closing (β) rate contants have nearly identical voltage sensitivities with a V_o of ±62 mV. The data presented in this study are not consistent with the contingent gating scheme (for two identical gates in series) proposed for other more V_j-dependent gap junctions and alternatively suggest that each gate responds to the applied V_j independently of the state (open or closed) of the other gate.

INTRODUCTION

Gap junctions mediate the electrical cell-to-cell communication necessary for synchronous impulse propagation and initiation of contraction in cardiac tissues (Page and Manjunath, 1986). Hexameric assembies of integral membrane proteins form hemichannels, or connexons, which align with connexons of an adjacent cell to form patent channels (Makowski et al., 1977). It is now generally accepted that there is a family of structurally related gap junction proteins, or connexins, that contain both highly conserved and unique primary amino acid sequences (Beyer et al., 1990). The different connexins have partially overlapping tissue distributions. Molecular cloning techniques and site-directed antibodies have identified close homologies of connexin43 as the predominant gap junction protein in a variety of species of mammalian heart (Beyer et al., 1987, 1989; Yancey et al., 1989; El Aoumari et al., 1990; Fishman et al., 1990). The best evidence that connexin43 forms junctional channels comes from the functional expression of this protein in paired *Xenopus* oocytes injected with rat connexin43 mRNA or in communication-deficient SKHep1 cells transfected with human connexin43 cDNA (Swenson et al., 1989; Werner et al., 1989; Fishman et al., 1990). Injection of rat connexin43 mRNA into *Xenopus* oocytes results in the formation of large junctional conductances (g_j) that are not sensitive to transjunctional potentials (V_j) of less than ±60 mV (Swenson et al., 1989; Werner et al., 1989). In these same studies, it was also observed that connexin43 is capable of forming hybrid channels with an endogenous V_j-sensitive connexin, presumably connexin38 (Ebihara et al., 1989). In paired cardiac myocytes from adult rat or guinea pig heart, g_j was found to be insensitive to transjunctional potentials (Kameyama, 1983; Metzger and Weingart, 1985; White et al., 1985; Weingart, 1986; Noma and Tsuboi, 1987; Rüdisüli and Weingart, 1989). This is contrary to observations in embryonic chick heart (Veenstra, 1990, 1991*a*), but these functional differences between species may be conferred by the presence of different connexins (Beyer et al., 1990; Veenstra 1991*a*).

Recently, Rook et al. (1988, 1990) have observed that newly formed gap junction channels between neonatal rat ventricular myocytes behave in a voltage-dependent manner when transjunctional voltage (V_j) exceeds ±50 mV. This V_j-dependent behavior was observed provided that $g_j < 1$ nS. Junctional currents attributable to the opening and closing of single gap channels have been detected in paired neonatal and adult mammalian cardiac myocytes with corresponding channel conductances of 32 or 50 pS (Burt and Spray, 1988; Rook et al., 1988, 1989; Rüdisüli and Weingart, 1989). These values agree closely with channel conductance values of 60 pS obtained in SKHep1 cells stably transfected with human connexin43 cDNA (Fishman et al., 1990, 1991).

Address correspondence to Dr. Veenstra.

0006-3495/92/07/139/13 $2.00

This study was undertaken to determine the precise relationship between transjunctional voltage and junctional conductance in mammalian cardiac gap junctions containing connexin43. We found that gap junctions of neonatal hamster ventricular myocardium stained specifically with antisera raised against a unique rat connexin43 peptide sequence. Unlike previous reports, cell pairs with a junctional conductance of 12 nS still exhibited a marked voltage-dependent gating when the transjunctional voltage exceeded ±50 mV which could be described by a two-state Boltzmann distribution. Preliminary observations of these results have been presented elsewhere (Veenstra, 1991*b*; Wang et al., 1991).

MATERIALS AND METHODS

Cell isolation and culture

Syrian hamsters were obtained from our breeding colony maintained in the Central Animal Care Facility at the State University of New York, Health Science Center at Syracuse. To prepare the primary heart cell cultures, myocytes were isolated from heart ventricles of 3-d neonatal Syrian hamsters. The animals were killed by cervical dislocation and the hearts immediately removed using sterile techniques. The extirpated hearts were washed twice in cold Hank's solution (Gibco Laboratories, Grand Island, NY) to remove residual blood. The ventricles were dissected free and minced into 1–2-mm^3 pieces using a new scalpel blade under a dissecting microscope. The pieces were washed twice with ice-cold Hank's solution, then treated with 0.08% trypsin and 0.01% collagenase in Hank's solution for 10 min at 37°C in an incubator with gentle agitation. The first supernatant was discarded and the supernatant from the next three cycles was diluted twofold with cold culture medium composed of Earle's MEM, 15% FCS, 200 mM glutamine, 100 U/ml penicillin, and 100 mg/ml streptomycin. Cells were harvested from the enzymatic solution by centrifugation, and the cell pellet was resuspended in fresh culture medium. The cell culture was enriched for myocytes by a differential adhesion step (Lemanski and Tu, 1983). The final density of cells was adjusted to $\approx 2 \times 10^5$ dispersed cells/ml of medium. The cells were grown on gelatin-coated glass coverslips in 35-mm-diam plastic culture dishes, and incubated at 37°C in a humidified atmosphere of 5% CO_2 and 95% air. The culture medium was changed every 48 h.

Fixation and immunofluorescent staining

Cells grown on coverslips for 2–5 d were removed from the culture dishes and washed three times with PBS (pH 7.4) composed of 0.15 M NaCl and 10 mM phosphate buffer. Cells were fixed and permeabilized in cold acetone for 30 s at −20°C. After 2 min of air drying at 22°C, the coverslips were washed again in PBS three times for 3 min each, then stored at 4°C in excess PBS. Rabbit antiserum against rat connexin43 amino acid residues 252–271 (courtesy of Dr. Eric C. Beyer, Washington University, St. Louis, MO) was used for primary staining of gap junction protein. A complex of biotinylated donkey anti-rabbit IgG secondary antibody (Lot #62) and Texas Red–streptavidin (Amersham Corp., Arlington Heights, IL) antibody, diluted in PBS, was used as a fluorescent marker for anti-connexin43 antibody.

After the coverslips with the attached cells were removed from the PBS, they were incubated for 15 min at 37°C in 3% filtered nonfat milk to block nonspecific staining. This was immediately followed by a 60-min incubation with anti-connexin43 diluted 1:40 with PBS. The cells were washed three times in PBS, blocked with 3% milk again, incubated with biotinylated anti-rabbit secondary antibody (1:20 dilution) in a humidified chamber at 37°C for 1 h or 4°C for overnight. The cells were then incubated with Texas Red–streptavidin at 37°C for 1 h or 4°C for overnight and washed with PBS. Cells were viewed with a light microscope (Universal; Carl Zeiss, Inc., Thornwood, NY) equipped with epifluorescent illumination using a mercury light source and photographed on Kodak plus-X film.

Junctional current and conductance measurements

All electrophysiology experiments were performed at room temperature according to previously published procedures (Veenstra and DeHaan, 1986; Veenstra, 1990). Plates of cultured myocytes were rinsed five to seven times with balanced salt solution (BSS, mM: 142 NaCl, 1.3 KCl, 0.8 $MgSO_4$, 0.9 NaH_2PO_4, 1.8 $CaCl_2$, 5.5 dextrose, and 10 HEPES, pH 7.2) and placed on the stage of an inverted phase contrast light microscope (IMT-2; Olympus Corp. of America, New Hyde Park, NY) for observation. GΩ seals were formed on each cell of a pair using patch pipettes with tip resistances of 4–6 MΩ when filled with standard internal pipette solution (IPS, mM: 110 Kglutamate, 15 NaCl, 1 KH_2PO_4, 4.6 $MgCl_2$–$6H_2O$, 5 EGTA, 3 Na_2ATP, 3 Na_2phosphocreatine, and 25 HEPES). Access to the cell interior was gained by the application of a pulse of suction. Whole-cell capacitive currents in response to a 10-mV depolarizing step (holding potential = −80 mV) were simultaneously recorded using a 1 MHz A/D board (RC Electronics, Inc., Santa Barbara, CA). Electrode resistances following patch beak were determined from the capacitive current transients of each cell as previously described (Veenstra and DeHaan, 1988). Settling time for the voltage clamp circuit was ≤800 μs. Whole-cell electrode resistances ranged from 14 to 34 MΩ (mean ± SEM: 20.1 ± 1.8 MΩ, $n = 16$). Cell input resistances ranged from 1 to 5 GΩ. Because series resistance was typically <3% of the cell input resistance, series resistance compensation was not used.

Junctional currents were measured directly under dual whole-cell patch-clamp conditions as previously described (Veenstra, 1990, 1991*a*). Briefly, a transjunctional voltage gradient (V_j) is applied by setting the command potentials (V_1 and V_2) to different values and measuring the whole cell currents (I_1 and I_2) produced under these conditions. This was accomplished by initially setting $V_1 = V_2 = -40$ mV for 5 s to determine the membrane holding current for each cell, followed by the application of a 2-s hyperpolarizing or depolarizing voltage pulse to cell 1 ($\Delta V_1 = -V_j$) while maintaining V_2 constant. During each ΔV_1 pulse, each patch-clamp amplifier will supply an additional whole-cell current (ΔI_1 and ΔI_2) to maintain V_1 and V_2 at their respective values. Junctional current (I_j) will be of opposite sign in the two cells because junctional resistance (R_j) is isolated from ground by the input resistance (R_{in}) of each cell (Veenstra and DeHaan, 1988). R_{in} is determined by the parallel combination of the seal resistance (R_s) and membrane resistance (R_m) of the cell. Any additional nonjunctional membrane currents will have the same sign in both cells because the direction of current flow is the same (from cell interior across R_{in} to ground) in this case. Only the change in I_2 (ΔI_2) during the ΔV_1 pulse is taken as a direct measure of I_j, whereas ΔI_1 equals the negative of I_j (relative to I_2) plus the capacitive and nonjunctional membrane currents (I_m) associated with the change in V_1. Junctional conductance (g_j) is calculated according to Ohm's law, or $g_j = I_j/V_j = -(\Delta I_2/\Delta V_1)$.

The accuracy of this conventional g_j measurement depends on two major assumptions: that $V_j = -\Delta V_1$ and that $I_j = \Delta I_2$. In actual terms, the membrane potential (V_m) for each cell differs from V by an amount equal to $-R_{el} \times I_m$ where R_{el} is the resistance of the patch electrode. Furthermore, it can be shown that $I_j = \Delta I_2 \times (1 + R_{el2}/R_{in2})$ (Rook et al., 1988, Giaume, 1991). So $g_j = [\Delta I_2 \times (1 + R_{el2}/R_{in2})]/[-\Delta V_1 - (\Delta I_2 \times R_{el2} - \Delta I_1 \times R_{el1})]$. The fraction of I_j that is absent from ΔI_2 must flow across R_{in2} to ground and therefore alter V_{m2}. The resulting change in V_{m2} can be expressed as $\Delta V_{m2} = I_j \times R_{c2}$ where $R_{c2} = (R_{in2} \times R_{el2})/(R_{in2} + R_{el2})$. It can also be shown that $\Delta V_{ml} = \Delta V_1/[1 + (R_{el1}/R_{in1}) \times [(R_{in1} + R_j + R_{c2})/(R_j + R_{c2})]$ where $R_j = 1/g_j$ and $V_j = \Delta V_{m2} - \Delta V_{m1}$. Hence, errors in estimating g_j will depend on the R_{el}/R_{in} and R_{in}/R_j. For the experiments presented in this study, $R_{el}/R_{in} < 3\%$

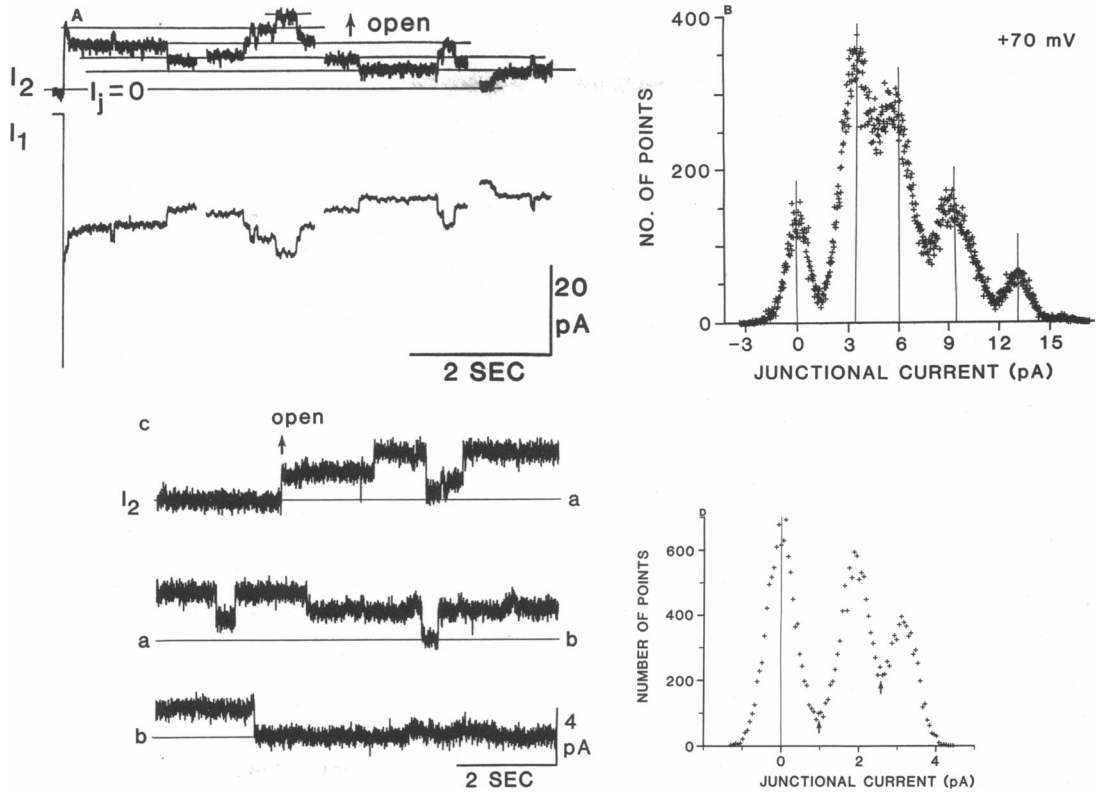

FIGURE 1 Junctional current measurements and channel amplitude histogram. (*A*) Whole-cell currents recorded under double whole-cell voltage-clamp conditions during a step in V_{m1} from 0 to −70 mV while V_{m2} was held constant at 0 mV. The zero junctional current level ($I_j = 0$) was set equal to the baseline current at $V_j = 0$ mV. Increasing junctional current is indicated by upward deflections in I_2 observed during the pulse (*arrow*). Note the presence of an active capacitive transient in I_1 during the onset of the pulse. The absence of this fast transient in I_2 is taken as an indication of adequate independent voltage control. The breaks in the traces correspond to 18.0-, 7.5-, and 23.8-s intervals that were omitted from the continuous 70-s current recording for the purpose of displaying data segments containing transitions to each current level. These records were low pass filtered at 200 Hz and digitized at 1 kHz. (*B*) Channel amplitude histogram of the gap junction channel activity shown in *A*. Each peak corresponds to the different current levels illustrated in *A* by the thin lines. Four peaks are clearly evident above the $I_j = 0$ baseline, whereas a fifth peak (above 15 pA) is poorly defined because the time duration (area under the peak) amounted to <1% of the cumulative recording time. The difference between successive peaks corresponds to the mean single channel current (i_j) for the observed activity. These values were 3.5 (n = 19 channel events), 2.6 (n = 129), 3.4 (n = 69), and 3.7 pA (n = 23), respectively (beginning with the first peak above baseline). (*C*) Junctional current record (ΔI_2) from a second cell pair during a +80-mV V_j step beginning at the arrow indicating the direction of channel openings. The thin horizontal line indicates the ground state (I_j = 0 pA), and the lowercase letters (*a* and *b*) indicate breaks made in the continuous 22-s record for display purposes only. (*D*) Amplitude histogram for the channel activity shown in *C*. The arrows point to the threshold levels used for detecting channel transitions. The mean single channel currents were 1.9 and 1.3 pA.

and $R_{c2} \cong R_{el2} \cong 20$ MΩ. Hence, $I_j = 1.03 \times \Delta I_2 \cong \Delta I_2$ and the errors in $V_j = \Delta V_1$ will be small unless I_j is large, a condition that would occur when R_j is low. Excluding those cell pairs where only gap junction channel activity was observed ($g_j < 0.5$ nS, n = 8 pairs), g_j ranged from 0.82 to 13.29 nS (7.16 ± 1.30 nS, mean ± SEM, n = 11 pairs). Under these conditions, $\Delta V_{m1}/\Delta V_1$ should range from 97 to 81%, respectively, from the lowest to the highest g_j pair (87 ± 0.3%, mean ± SEM).

A brief example of paired whole-cell currents is illustrated in Fig. 1 *A*. I_j is observed as upward deflections in I_2 and the $I_j = 0$ refers to the membrane holding current obtained when $V_{m1} = V_{m2}$ (=0 mV in this case). Transient capacitive and constant background currents are evident in I_1 and absent in I_2 during the −70-mV V_j pulse. In this cell pair, discrete quantal changes in I_j, which correspond to the opening and closing of individual gap junction channels, are evident because of the low junctional conductance ($g_j < 0.3$ nS). Quantitative measurement of I_j is performed by constructing a current amplitude histogram of the digitized I_2 signal as presented in Fig. 1 *B* (Veenstra, 1990). All I_j and g_j measurements are obtained by taking the differences between the means of each Gaussian peak in the histogram. There are five prominent peaks in Fig. 1 *B* and a barely discernible sixth peak above 15 pA. Each peak corresponds to one of the six discrete levels indicated by the solid lines in Fig. 1 *A*, and the area under each peak is proportional to the time spent in each state (level). Single-channel currents (i_j) are taken as the difference between the means of two adjacent peaks and the single-channel conductance (γ_j) can be calculated accordingly ($\gamma_j = i_j/V_j$). Beginning with the first channel above baseline in Fig. 1 *B*, γ_j equals 50, 37, 49, and 52 pS, respectively.

In three experiments, resolution of channel currents of ≤2 pA could be resolved. The channel activity shown in Fig. 1 *C* was obtained from a different cell pair under identical experimental conditions. The arrow indicates the direction of open-channel currents observed with the onset of a +80-mV V_j pulse, which remained on for the remainder of the 22-s continuous current record displayed in this panel. The amplitude histogram is shown in Fig. 1 *D* and the channel currents measured 1.9 and 1.3 pA, or γ_j = 24 and 16 pS. Channel events are counted by setting a threshold detector equal to the valley between adjacent peaks in the amplitude histogram and scanning the I_2 trace a second time. Threshold levels for counting channel events are optimally >2 SD from the mean of each peak. Only events with a duration ≥ 5 points (=5 ms) are counted as an event. For the example shown here, 44 transitions

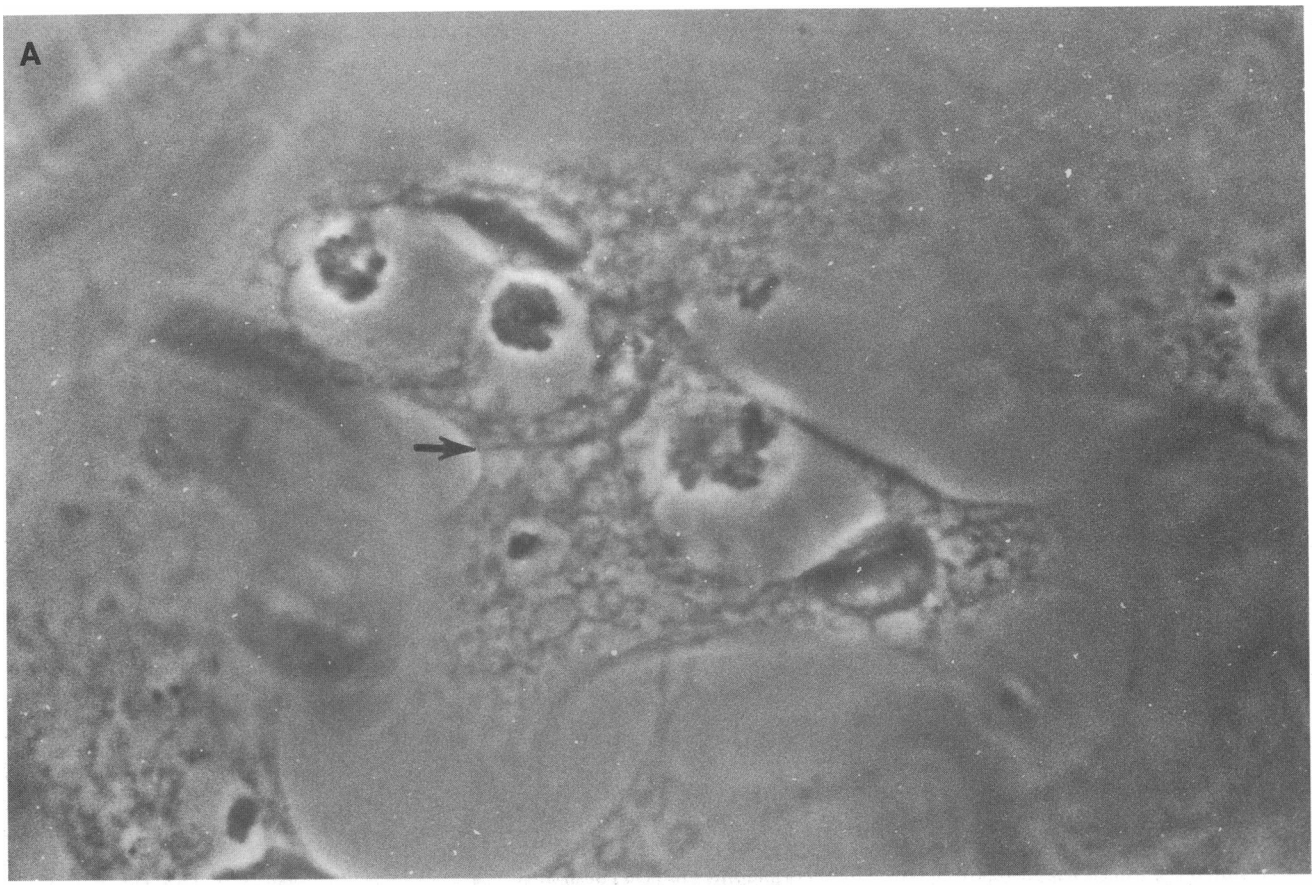
A


B

were detected, omitting the initial step associated with the onset of the pulse. These procedures were followed for all experiments presented in this manuscript.

RESULTS

Immunohistochemical localization of gap junctions in vitro

After 1–2 d in vitro, cardiac myocytes appear round in shape (few cytoplasmic projections) compared to fibroblasts, which spread out more rapidly in culture (Li and Lemanski, 1990). To determine if 3-d neonatal hamster cardiac myocytes express connexin43 in vitro, cultured ventricular myocytes were stained with anti–connexin43 252–271 antiserum (Beyer et al., 1989) using standard immunohistochemical techniques. Fig. 2 displays a phase contrast micrograph and immunofluorescent image of such a cardiac myocyte cell pair. In both micrographs, the arrow indicates the location of intercellular contacts between the two cells. Punctate labeling of the intercellular surface with anti–connexin43 antisera is evident in Fig. 2 *B*. Some cell clusters, presumably containing fibroblasts, did not stain with the connexin43 antiserum.

Regulation of junctional current by transjunctional potentials

To assess the relationship between transjunctional voltage and junctional current, V_j was varied between the values of ±100 mV by systematically altering the membrane voltage of one cell (V_{m1}) from a common holding potential of −40 mV in 10-mV increments. Every 2-s-duration V_j pulse was separated by a 5-s recovery interval (V_j = 0 mV). Representative currents from one neonatal hamster cell pair are presented in Fig. 3 *A*. Instantaneous I_j, measured as the change in I_2 during the first 10 ms of each V_j pulse, increases linearly with V_j of either polarity. Beyond ±50 mV, I_j undergoes a time- and V_j-dependent decay to new steady-state values. Both instantaneous and steady-state I_j values are plotted as a function of V_j in Fig. 3 *B*. The instantaneous I_j–V_j relationship, illustrated by the open squares, was linear, with the slope of the line being equal to g_j of the preparation (12.23 nS). Steady-state I_j, illustrated by the open diamonds in Fig. 3 *B*, was virtually identical to instantaneous I_j in the −40 to +50-mV range, but deviates from linearity with further increases in V_j. Beyond ±70 mV, steady-state I_j actually diminishes with increasing V_j, thus producing a negative slope conductance for the junctional membrane. Similar results were obtained from 11 other cell pairs where g_j ranged from 0.82 to 13.29 nS (7.16 ± 1.30 nS, mean ± SEM). In three additional cell pairs, where g_j of 36 to 40 nS were calculated from the slope of the linear instantaneous I_j–V_j relationships (data not shown), steady-state I_j had declined by <10% at V_j of ±80 mV and steady-state I_j was reduced by an average of only 15% from instantaneous I_j values at V_j = ±100 mV. In these three experiments, the measured R_j of only 25–28 MΩ corresponds to the lower limit for the sum of R_{el1} and R_{el2}. Under these conditions, $\Delta V_{m1}/\Delta V_1 \cong 0.75$ and I_j = 3.6–4.0 nA at 100 mV results in a ΔV_{m2} of 40–50 mV. Hence, V_j will equal only 25–35% of ΔV_1 and very little time- and voltage-dependent decay would be expected to be observed under these circumstances.

The time course of the decline in I_j was also examined at each V_j above ±60 mV by fitting exponential functions to the decay phase of each I_j trace. Accurate fits were obtained in eight experiments. Examples of the monoexponential fits obtained from one of these cell pairs are illustrated in Fig. 4. The corresponding V_j is indicated to the left of each trace, and the smooth line represents the monoexponential fit of the data. There was close agreement between the theoretical curves and experimental data at all voltages examined regarding both the rate of decay and steady-state I_j. In some I_j traces, a fast component (τ < 40 ms) was also observed. Predicted steady-state I_j values, determined by extrapolating the idealized fit to pulse durations of $\tau \rightarrow \infty$, varied by no more than 5% from the steady-state I_j measured at the end of a 2-s pulse in 62 of 64 trials. The monoexponential time constants for all eight experiments are summarized in Table 1. There was a large amount of scatter from one experiment to the next, as indicated by the large SEM observed at V_j < ±100 mV. Decay time constants decreased as V_j increased in either direction, consistent with previous observations in other V_j-dependent cardiac gap junctions (Veenstra, 1990, 1991*a*).

Because I_j undergoes a time-dependent decay at large potentials, experiments were performed to determine the rate of recovery from inactivating potentials. For these experiments, the recovery interval between inacti-

FIGURE 2 Immunofluorescence photomicrographs of connexin43 in cultured neonatal hamster myocytes. (*A*) Phase contrast image of neonatal hamster ventricular myocytes cultured for 2 d in vitro. The arrow indicates the location of an extensive zone of intercellular contacts between two cells. ×1,378. (*B*) Immunofluorescent image of the same field obtained with an antibody generated to amino acid residues 252–271 of rat connexin43. Cultured myocytes were permeabilized with cold acetone before exposure to anti–connexin43 252–271 antibody. Bound antibody was detected by treating washed cells using a biotinylated goat anti–rabbit IgG conjugated to Texas Red–streptavidin. Punctate staining, indicative of the presence of connexin43 in the gap junctions of this preparation, is observed at the intercellular contact zones between the two cells. Faint nuclear staining is also present, but much fainter than at the intercellular surface. Background fluorescence was not detectable in control cells treated with only the biotynilated goat anti–rabbit IgG/Texas Red–streptavidin conjugate (data not shown).

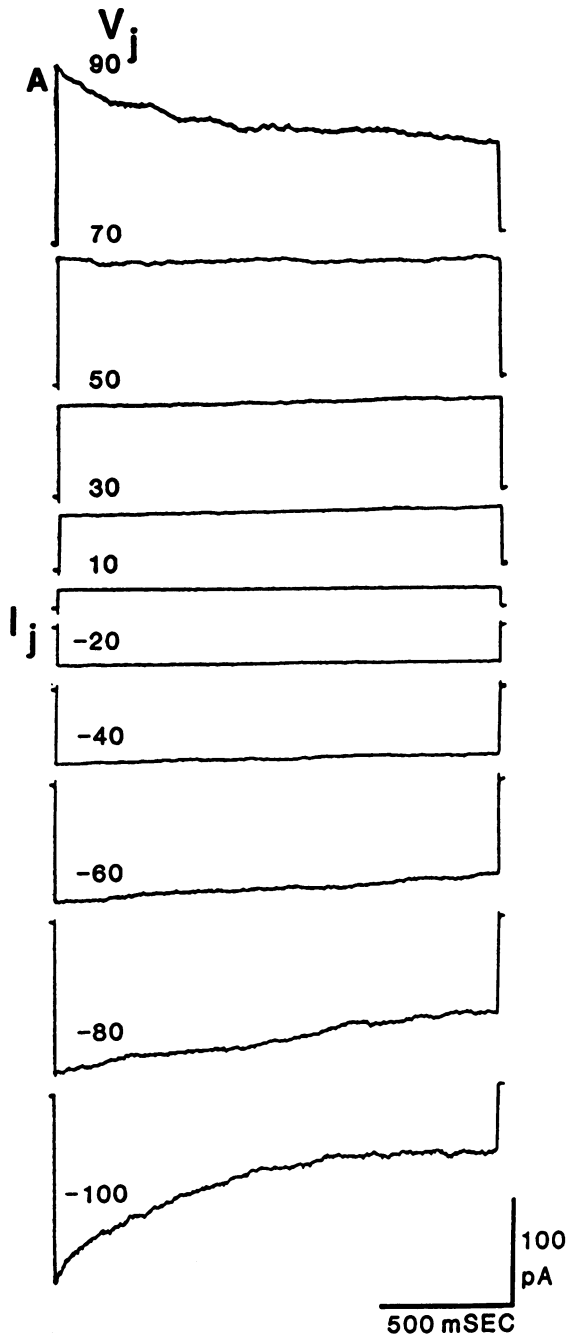

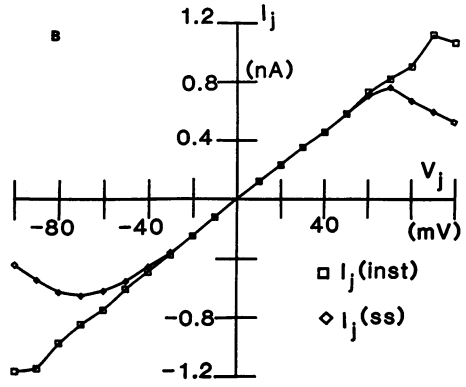

vating (2-s duration, 80 mV) V_j pulses was varied from 100 ms to 10 s. Instantaneous I_j measurements were obtained at V_j = 20 and 80 mV by immediately preceding each 80-mV V_j pulse with a 20-mV, 100-ms prepulse. The purpose of the prepulse was to provide a measurement of g_j immediately before stepping to an inactivating potential. In three experiments, instantaneous g_j measured at both potentials was identical. This observation, along with the linear instantaneous I_j–V_j relationship (Fig. 3), confirms that the time-dependent relaxation of I_j does not occur until large V_j values (>50 mV) are achieved. The time course for the recovery of g_j from inactivating potentials was achieved by normalizing g_j (normalized g_j = G_j) for each experiment to the value obtained after a 10-s recovery interval. G_j was then plotted as a function of the recovery interval, as illustrated in Fig. 5, and fitted with an exponential function of the form $G_j = 1/[1 + \exp(-t/\tau)]$ to determine the recovery time constant of ~300 ms.

Because the inactivation and recovery of I_j are time-dependent processes, it was of interest to examine the effects of instantaneous polarity reversal on I_j. In four experiments, I_j was recorded from a cell pair during 80-mV V_j steps, which were given alone or preceded by a prepulse of equal duration (2 s), opposite polarity, and varying amplitude. The results of one experiment are shown in Fig. 6. The top trace (*top panel*) illustrates the control response to a +80-mV test pulse. When the test pulse is preceded by an opposite-polarity prepulse of sufficient magnitude to inactivate I_j by 74% (*bottom trace*, V_j = −80 mV), there is still a transient rise in I_j immediately upon polarity reversal to within 81% of the control response. Prepulses to intermediate V_j values, such as −40 mV, failed to produce much inactivation of I_j and reduced the instantaneous I_j of the +80-mV test pulse by only 5% (data not shown). Similar results were observed in all four experiments, indicating that g_j increases rapidly before inactivating in response to the reversal of a large V_j gradient. The exponential decay constants (τ) for the control responses averaged 246 ± 34 ms (mean ± SEM, n = 4), whereas the same values for the −80-mV prepulse test responses were 305 ± 27 ms. These values were not significantly different ($P > 0.15$, paired t test). The current flowing during the test response was not observed to overshoot the currents during a control re-

FIGURE 3 Voltage dependence of neonatal hamster cardiac gap junctions. (*A*) Junctional current (I_j) during a 2-s pulse to the indicated transjunctional voltages (V_j) undergoes a time-dependent decay when V_j exceeds ±50 mV. Instantaneous (onset of pulse) junctional conductance (g_j) values ranged from 10.64 to 12.80 nS and steady-state (end of pulse) g_j values ranged from 4.49 to 12.20 nS for the current traces shown. (*B*) Instantaneous (*inst*) and steady-state (*ss*) I_j for the experiment shown in Fig. 3 *A* were plotted as a function of V_j. The instantaneous I_j–V_j relationship approximates a straight line with a slope of 12.23 nS. The steady-state I_j–V_j relationship deviates from linearity above ±50 mV and has a negative slope above ±70 mV. The lines connecting the data points were drawn by eye.

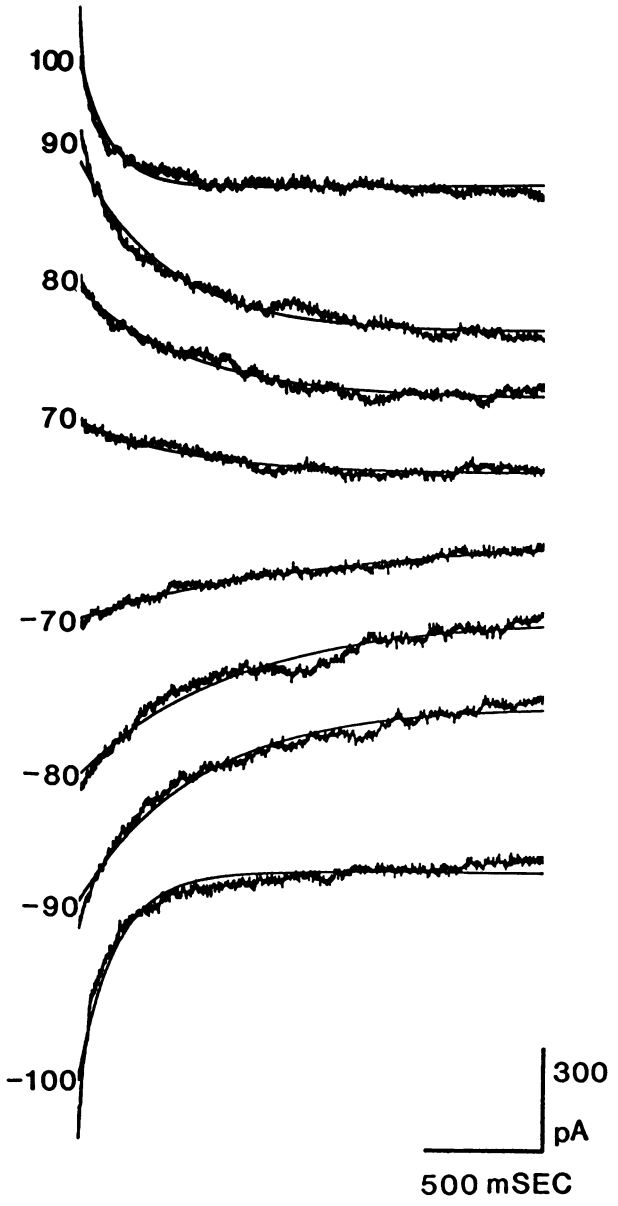

FIGURE 4 Decay time constants of junctional current. The smooth line depicts the best fit of the decay phase of each I_j trace recorded at the indicated V_j (*left margin*). Time constants for the traces are (mV, ms): +100, 131; +90, 387; +80, 504; +70, 472; −70, 1,089; −80, 694; −90, 524; −100, 169.

sponse in any of the experiments, a finding contrary to earlier observations from V_j-dependent gap junctions between amphibian blastomeres (Harris et al., 1981).

Steady-state junctional conductance–voltage relationship

To assess the relationship between steady-state g_j (g_{ss}) and V_j, g_{ss} was normalized to the instantaneous g_j (g_{inst}) of each pulse and the results of eight experiments were pooled together. Because the instantaneous I_j–V_j relationships were always linearly related, this provided a convenient method for normalizing the data from cell pairs having different g_j values. The results of eight experiments are summarized in Fig. 7. Normalized g_{ss} (G_{ss}) ranged from 0.80 to 1.0 for $0 \leq V_j \leq \pm 50$ mV and declined to a minimum value of 0.32–0.34 at ±100 mV. For each polarity, the G_{ss}–V_j curve was fit by a Boltzmann equation of the form:

$$G_{ss} = \{(G_{max} - G_{min})/[1 + \exp(A(V_j - V_o))]\} + G_{min}, \quad (1)$$

where G_{max} is the normalized maximum conductance (= 1), G_{min} is the normalized minimum conductance for large transjunctional voltages, V_o is the voltage where G_{ss} lies halfway between G_{max} and G_{min}, and A is a parameter expressing the slope of the curve (Spray et al., 1981). The constant A can be expressed as zq/kT, where z is the valence of charge q that act as the voltage sensor in the membrane to effect the transition from the open to closed conductance states, and kT represent Boltzmann's constant and absolute temperature, respectively. For the negative polarities shown Fig. 7, $G_{min} = 0.34$, $A = -0.112$ (which corresponds to a valence of 2.8 electrons), and $V_o = -69$ mV. For the positive polarites, $G_{min} = 0.32$, $A = 0.093$ ($z = 2.4$), and $V_o = +61$ mV.

Behavior of gap junction channels

In eight additional experiments, gap junction channel currents were resolved owing to the low g_j of these cell pairs. Complete single gap junction channel current-voltage (i_j–V_j) relationships were determined in two of these eight experiments either by applying the voltage protocol described in Fig. 3 or by manually reproducing each V_j step to increase the pulse duration (and the number of channel events). The results of these two experiments are illustrated in Fig. 8. Channel openings are clearly evident in Fig. 8, *A* and *C*, as upward deflections in i_j when V_j is positive and downward deflections in i_j when V_j is reversed. As V_j approaches 0 mV, i_j decreases in amplitude and approaches the noise limit of the recordings. Thus, channel amplitudes were determined only in the range of ±50 to ±100 mV. Fig. 8 *A* illustrates the channel activity observed during brief 2-s duration pulses to the indicated V_j. The amplitudes of the channel currents, determined using the procedures illustrated in Fig. 1 on 40–70-s continuous recording intervals, are plotted as individual points on the V_j axis in Fig. 8 *B*. The solid line represents the best fit of the data as determined by the least-means-square criterion. Linear regression analysis produced identical results ($r = 0.96$). The straight line has a slope of 46 ± 2 pS, which is consistent with the single-channel conductance values (γ_j) reported for mammalian cardiac gap junction channels (Burt and Spray, 1988; Rook et al., 1988; Rüdisüli and Weingart, 1989). Similar results were obtained in the ±80 to ±100-mV range from four other cell pairs (Veenstra, 1991*b*). Fig. 8, *C* and *D*, represents the gap junction

TABLE 1 **Average decay time constants of junctional current**

	V_j									
	mV									
	−100	−90	−80	−70	−60	60	70	80	90	100
τ, ms	151	251	451	687	1101	1049	563	432	198	100
SEM	17	62	64	248	506	190	58	137	41	18
n	7	8	8	8	6	6	8	8	8	7

channel activity and i_j–V_j relationship obtained from a different cell pair using the same procedures. In this example, only 2-s-duration pulses were analyzed, so the event count is smaller than for the previous experiment. The slope of the linear i_j–V_j relationship was 33 ± 2 pS (r = 0.95). Single channel conductances of 25–35 pS were observed in two other experiments when $\pm 80 \leq V_j \leq \pm 100$ mV. Many of the I_j traces in Fig. 8, *A* and *C*, reveal the closure of one or more channels during the first 500 ms of the V_j pulse, which indicates that the time-dependent decrease in I_j may be due to the V_j-dependent closure of gap junction channels.

Channel gating rate constants

It is possible to calculate the channel opening and closing rate constants from the G_{ss} values and first-order decay time constants presented in Figs. 4 and 7 and Table 1, assuming that the channel transitions between the open and closed states are due to the free energy difference (which varies as a function of transjunctional voltage) between the states (Harris et al., 1981). For the reaction scheme:

$$\text{open} \underset{\beta}{\overset{\alpha}{\rightleftharpoons}} \text{closed}.$$

α and β can be calculated from the decay time constant τ and the normalized steady-state G_{ss} according to the following equations:

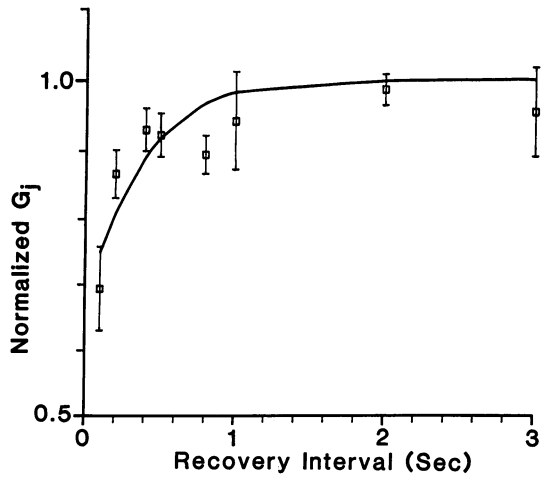

FIGURE 5 Time-dependent recovery of gap junctional conductance. The recovery interval between +80 mV V_j pulses (2-s duration) was varied from 100 ms to 10 s in three cell pairs. For each experiment, instantaneous g_j values were plotted as a function of recovery interval by normalizing g_j to the value obtained with a 10-s recovery interval. Each point represents the mean G_j (±SEM) and the solid line is a theoretical fit obtained using the equation $G_j = 1/[1 + \exp(-t/\tau)]$, where τ = 297 ms. All data points between 3 and 10 s were within ±1 SEM of the normalized maximum G_j (=1).

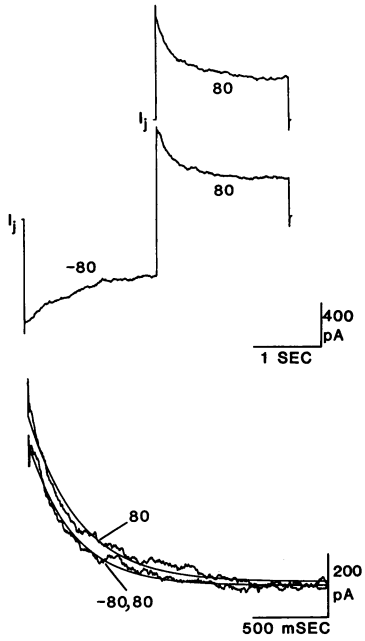

FIGURE 6 Transient recovery of I_j from inactivation upon polarity reversal. The control +80-mV V_j pulse (*top panel, first trace*) was preceded by a time interval where both cells were clamped to a common holding potential of −40 mV while the test +80-mV V_j pulse (*top panel, second trace*) was preceeded by 2-s prepulse to V_j = −80 mV. The decay phases of the same two traces are superimposed in the bottom panel for comparison. For the control pulse, instantaneous I_j was 350 pA (g_{inst} = 4.38 nS) and decayed to a steady-state I_j of 126 pA (g_{SS} = 1.58 nS) with a time constant (τ) of 335 ms. After inactivation at −80 mV (*bottom panel*), instantaneous and steady-state I_j still peaked at 284 and 113 pA (g_{inst} = 3.55 nS and g_{SS} = 1.41 nS) and τ = 294 ms. Note that I_j during the test pulse does not overshoot the control pulse.

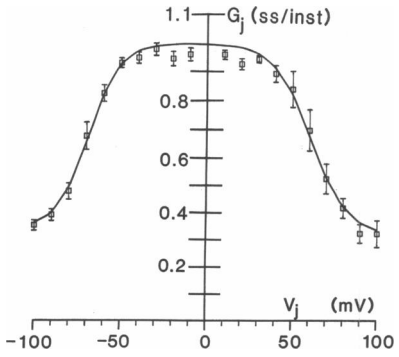

FIGURE 7 Steady-state junctional conductance–voltage relationship. Ratio of steady-state (*ss*) to instantaneous (*inst*) g_j taken from eight different cell pairs. Each point represents the mean ± SEM. G_{ss} declines with increasing V_j in either direction with the greatest decrease in G_{ss} occurring when V_j exceeds ±50 mV. The solid line is a theoretical fit of the data assuming a two-state Boltzmann distribution (see text) with G_{min} = 0.34 and 0.32, A = −0.112 and 0.093, and V_o = −69 and +61 mV for negative and positive V_j, respectively.

$$\alpha = G_v/\tau \tag{2}$$

and

$$\beta = (1 - G_v)/\tau, \tag{3}$$

where $G_v = G_{ss} - G_{min}$. Using these equations, α and β were calculated from the mean G_{ss} and τ values presented in Fig. 7 and Table 1. The closing rate constant (β) was observed to be higher than α at large V_j values ($V_j > V_o$). This is similar to the findings reported for other V_j-dependent gap junctions (Harris et al., 1981). The solid lines in Fig. 9 represent the best fit of the data according to the equations:

$$\alpha = \lambda \exp[A_\alpha(V - V_o)] \tag{4}$$

and

$$\beta = \lambda \exp[A_\beta(V - V_o)], \tag{5}$$

where λ is a constant equal to the rate when $\alpha = \beta$, which occurs at $V = V_o$. A_α and A_β are the respective voltage sensitivities of the opening and closing rates. For the curves shown in Fig. 9, λ = 0.69 and 0.67, A_α = −0.06 and 0.04, A_β = −0.06 and 0.07, and V_o = −63 and +62 mV for the negative and positive voltages, respectively. τ was calculated from Eqs. 4 and 5 as $1/(\alpha + \beta)$ and produced predicted decay constants of (mV, ms): −100, 148; −90, 262; −80, 437; −70, 635; −60, 739; 60, 750; 70, 628; 80, 381; 90, 200; 100, 100. These values agree closely with the values presented in Table 1 except for ±60 mV. G_{ss} was also calculated using the equation $G_{ss} = (G_{max} - G_{min}) \times (\alpha/(\alpha + \beta))] + G_{min}$ and produced a curve nearly identical to the Boltzmann curve in Fig. 7 (data not shown). The term $[\alpha/(\alpha + \beta)]$ is equivalent to the steady-state open probability for the V_j-sensitive conductance.

DISCUSSION

Unitary channel conductance

The slope conductances of linear single gap junction channel current-voltage relationships provide reliable estimates of the mean gap junction channel conductances observed in low g_j cell pairs. In paired neonatal hamster ventricular myocytes, we observed linear slope conductances of 33 ± 2 and 46 ± 2 pS (Fig. 8). Similar gap junction channel conductance (γ_j) values of 20–30 and 39–60 pS have been obtained from neonatal rat and adult guinea pig myocyte pairs (Rook et al., 1988, 1989; Burt and Spray, 1988; Rüdisüli and Weingart, 1989) and immunocytochemical studies have revealed the presence of connexin43 in the junctional membranes of all adult mammalian ventricular myocytes in situ (Beyer et al., 1989; Yancey et al., 1989; El Aoumari et al., 1990) and in paired neonatal mammalian myocytes in vitro (Fig. 2; Laird and Revel, 1990). Based on the numerous channel conductance measurements from these preparations, it is generally agreed that a 40–60-pS channel is formed by connexin43. This concurs with the observation of a 60-pS channel following the transfection of SKHep1 cells with human connexin43 cDNA (Fishman et al., 1990, 1991).

In neonatal rat, a 30-pS channel conductance was attributed to the formation of heterologous fibroblast–myocyte gap junctions (Rook et al., 1989). Connexin43 is known to form heterologous gap junctions with connexin32 and connexin38 when expressed in Xenopus oocytes (Swenson et al., 1989; Werner et al., 1989). The formation of heterologous gap junctions could explain our observation of a 30-pS channel in three cell pairs (Fig. 8, *C* and *D*), although we cannot definitively confirm the identity of a fibroblast in these cases. Based on the observations of contractile activity and the extent of cell spreading during the first 24 h in culture, we estimate that >80% of the cells we recorded from were myocytes. We also cannot rule out the possibility that a 30-pS channel is due to the presence of other connexins, as observed in embryonic chick heart and liver hepatocytes (Zhang and Nicholson, 1989; Beyer et al., 1990), or that it is a subconductance state of a 60-pS channel. However, identification of a subconductance state requires the observation of the substate only in the presence of the larger channel (Fox, 1987), which was not observed for the experiment presented in Fig. 8, *C* and *D*. Recently, Kanter et al. (1992) have demonstrated the presence of mammalian homologs to chick connexin42 and connexin45 (named dog connexin40 and connexin45) in canine ventricular myocytes at the protein level. Chick connexin45 reportedly forms a 30-pS channel (Veenstra et al., 1992). In SKHep1 cells, low levels of endogenous coupling were manifested by the presence of a 30-pS channel, which was not identified by antibodies to con-

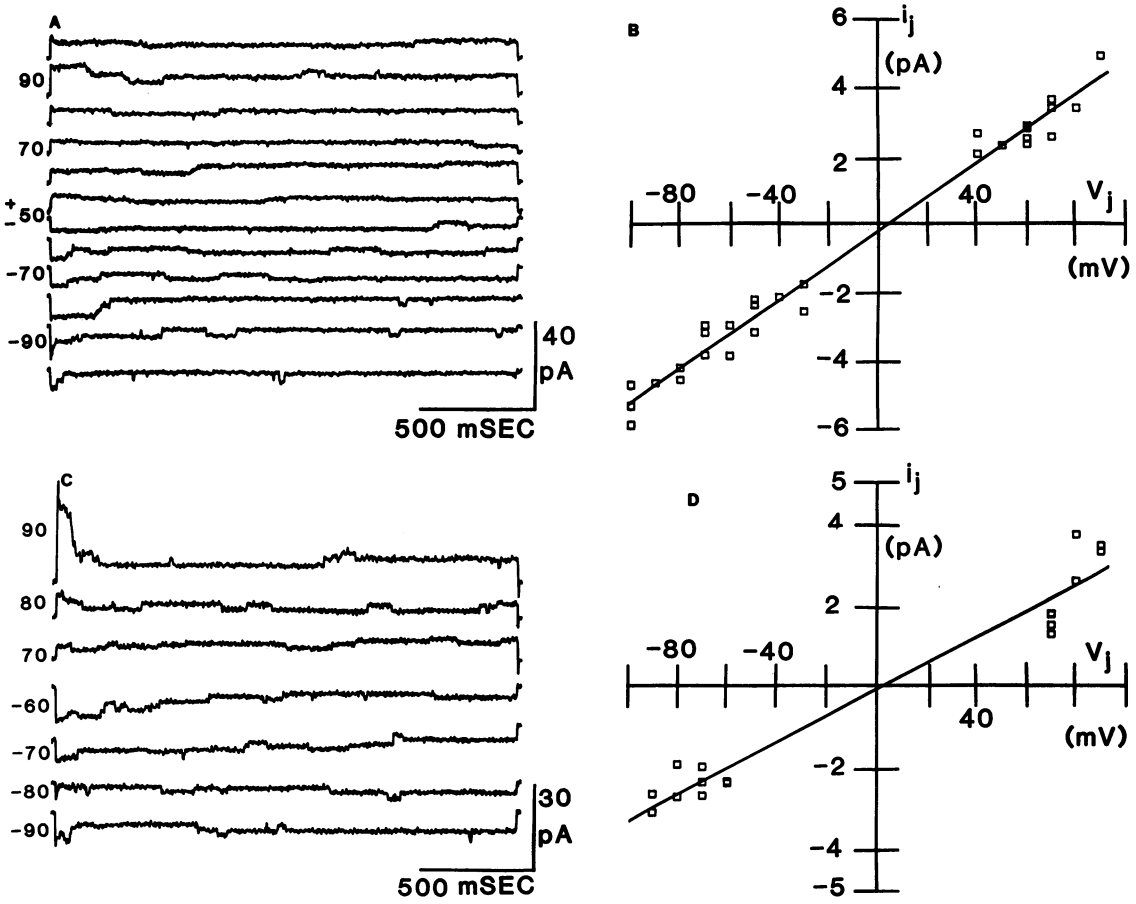

FIGURE 8 Single gap junction channel current–voltage relationships. (*A*) Gap junction channel activity recorded during 2-s pulses to the indicated V_j. Analog low pass filter frequency = 125 Hz and digital sample rate = 1 kHz. (*B*) Each point represents the current amplitude as determined from a current amplitude histogram compiled from 40–70 s of recording time. Number of channel events at each V_j ranged from 38 to 440. The solid line is a linear fit of the data with a slope of 46 ± 2 pS. (*C*) Gap junction channel activity from a different cell pair under identical experimental conditions. (*D*) Each point represents the current amplitude as determined from the current amplitude histogram compiled from each 2-s pulse. Number of observed channel events at each V_j ranged from 5 to 19. The solid line is a linear fit of the data with a slope of 33 ± 2 pS.

nexins26, -32, or -43 (Eghbali et al., 1990). The identification and functional expression of individual cardiac myocyte and fibroblast connexins by stable transfection in mammalian cell lines should provide the best method for determining the conductance properties of the connexin proteins.

Effects of transjunctional potential on junctional currents

In this investigation, the V_j dependence of mammalian cardiac gap junctions between paired 3-d neonatal hamster ventricular myocytes was quantitatively assessed. The results indicated a symmetrical drop in G_{ss} above V_j values of ±50 mV and are suggestive of a bilateral voltage-gated mechanism. The time-dependent decay and recovery processes followed first-order kinetics with time constants of similar dimensions. These observations are contrary to earlier studies in paired adult cardiac myocytes, although one explanation for the observed differences is that V_j did not exceed ±50 mV in many of the previous experiments (Kameyama, 1983; White et al., 1985; Weingart, 1986). A second explanation for the apparent lack of voltage dependence is that the large g_j of adult myocyte preparations precludes the observation of V_j-dependent behavior due to reductions in the actual applied V_j gradient, as was observed in three experiments in this study where calculated $g_j > 36$ nS. This occurs as the junctional resistance approaches the values of the electrode and cytoplasmic access resistances, thereby reducing the transjunctional voltage sensed by the gap junction channels. In the neonatal rat, Rook et al. (1988) did observe V_j-dependent behavior when $g_j <$ 1 nS and $V_j > \pm 50$ mV, but V_j sensitivity was not observed when g_j exceeded 1 nS in the same cell pair. They attributed this phenomenon to an increasing cytoplasmic voltage drop as gap junction plaques increase in size (Jongsma et al., 1991). Our findings indicate that the V_j sensitivity was still readily observed in cell pairs with G_j of 12 nS (Fig. 3), whereas a gradual loss of V_j sensitivity occurred somewhere between 12 and 36 nS. One likely explanation for the observed difference in these two neonatal preparations is that the access resistances of the

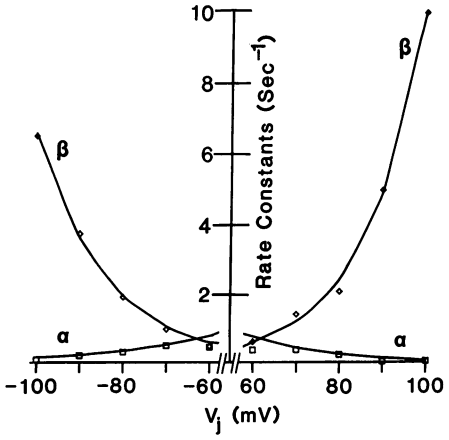

FIGURE 9 Voltage dependence of opening and closing rate constants. The open squares and diamonds represent the experimentally derived opening (α) and closing (β) rate constants calculated using Eqs. 2 and 3. The solid lines are the theoretical fit of the data using Eqs. 4 and 5. The experimental and theoretical values are in close agreement except for α at ±60 mV.

electrodes used in the present study varied from 14 to 34 MΩ (after membrane disruption, mean = 20 MΩ) compared to 20–100 MΩ for the studies in neonatal rat heart (Rook et al., 1988, 1990). If we assume that R_{in} = 1 GΩ, an R_{el} of 100 MΩ translates into a $\Delta I_2/I_j$ = 0.91 and a $\Delta V_{m1}/\Delta V_1$ = 0.67; and ΔV_{m2} will be approximately five times higher for a given I_j compared to R_{el} = 20 MΩ. Taking these three factors into consideration, a ΔI_2 of only 200 pA obtained during a ΔV_1 pulse of 100 mV (estimated g_j = 2 nS) will yield a true V_j of ~50 mV. From the Boltzmann curve presented in Fig. 7, $G_{ss} \cong$ 0.84–0.93 at ±50 mV. Hence, very little time- and voltage-dependent behavior would be observed under these conditions and, correcting for the errors in the V_j and I_j measurements, the actual $g_j \cong$ 4.7 nS. Based on these calculations, the observed V_j-dependent behavior appears to be an intrinsic property of the gap junctions that can be masked experimentally by the series resistance of the electrode. This interpretation is substantiated by the recent demonstration that human connexin43, expressed in SKHep1 cells, is moderately V_j sensitive with $G_{ss} \cong$ 0.80 at 50 mV and declines more rapidly beyond this point (Fishman et al., 1991).

What is the mechanism by which g_j is reduced when V_j exceeds ±50 mV between mammalian cardiac myocyte pairs? Single gap junction channel current–voltage relationships in adult guinea pig (Rüdisüli and Weingart, 1989) and neonatal hamster (Fig. 8) ventricular myocyte pairs are linear, with slope conductances of 39–50 pS. If the unitary channel conductance and the number of channels in the membrane remain constant, then V_j-dependent changes in g_j must be manifested as changes in the channel-gating properties. Reductions in the dwell time of multiple channel openings (area under each peak in a channel amplitude histogram) with increasing V_j, as observed in one neonatal hamster cell pair, are suggestive of such a mechanism (Veenstra, 1991*c*). Furthermore, ensemble averaging of 5–10 gap junction channel current traces produces an exponential decay in I_j similar to observed macroscopic currents from higher conductance gap junctions of similar origin (Rook et al., 1988; Veenstra, 1990, 1991*a*). Based on the observed V_j-dependent behavior, Rook et al. (1988) predicted the channel open-state probability (P_o) to vary from ~0.25 at V_j = ±100 mV to near 0.85 at ±50 mV. From the Boltzmann distribution presented in Fig. 7, G_{ss} equals 0.84–0.93 at V_j = ±50 and 0.32–0.34 at ±100 mV. Because $P_o = \alpha/(\alpha + \beta)$ in the steady state, we can obtain estimates of P_o at each voltage from the kinetic analysis presented in Fig. 9. Our calculations predict a maximum P_o of 1.0 at V_j = 0 mV and ~0.80 at V_j = ±50 and a minimum P_o near zero at V_j = ±100 mV. These estimates were based on the presence of only a single population of channels with simple two-state gating kinetics. Of course, this is only a $P_o(V_j)$ term, which applies to the already open channel, so the actual P_o for all gap junction channels could still be much less than 1.0 at low V_j values because other factors may cause some gap junction channels to be closed at rest (V_j = 0 mV). This interpretation is slightly different from previous correlative electrophysiological and morphological studies in neonatal rat heart, where it was suggested that virtually all channels are open at rest (Rook et al., 1990).

Kinetic considerations

Calculation of the theoretical time constants according to the relation $\tau = 1/(\alpha + \beta)$, where α and β are determined by the Boltzmann relations presented in Eqs. 4 and 5, produced values of ~100–150, 200–260, 380–440, 620–640, and 740–750 ms for V_j = ±100, ±90, ±80, ±70, and ±60 mV, respectively. These values are in reasonable agreement with the experimental values presented in Table 1, as are the experimental and theoretical rate constants presented in Fig. 9, with the possible exception of ±60 mV. The discrepancies between the experimental and theoretical values at ±60 mV may result from the difficulty in obtaining an accurate fit of decay constants >700 ms from 2-s-duration pulses. Overall, the two-state Boltzmann model, originally described for V_j-dependent gap junctions between amphibian blastomeres (Harris et al., 1981; Spray et al., 1981), provides an accurate description of the equilibrium and kinetic properties of V_j-dependent mammalian cardiac gap junctions. In contrast to the findings in amphibian blastomeres, the slope factors A_β and A_α are nearly identical. Because $\alpha > \beta$ in any first-order system when $V_j < V_o$ and vice versa, P_o is higher at low V_j values. In cardiac gap junctions, β is twice α at 100 mV, whereas α is 10 times greater than β at 0 mV.

The transient recovery of I_j after polarity reversal re-

veals further information about the gating behavior of the gap junction channels. Alternative models for the gating behavior of two gates in series with each other were advanced by Harris et al. (1981). The contingent and independent gating models both account for a transient rise in I_j upon polarity reversal with one major difference. The contingent gating model requires that the closed gate of the polarized channel must open before the other gate in series can respond to the transjunctional voltage. This hypothesis is schematically represented as

$$C_1O_2 \underset{\beta_1}{\overset{\alpha_1}{\rightleftharpoons}} O_1O_2 \underset{\beta_2}{\overset{\alpha_2}{\rightleftharpoons}} O_1C_2.$$

With the contingent gating model, overshooting junctional currents were produced during a given transjunctional voltage pulse when preceded by prepulses of opposite polarity. According to the independent gating model, junctional currents elicited during a V_j pulse preceeded by a prepulse of opposite polarity do not overshoot junctional currents elicited by the same V_j pulse in the absence of a prepulse. This model assumes that the gating of each gate by the applied voltage field occurs independently of whether the other gate is open or closed (Harris et al., 1981). In the experiment presented in Fig. 6, we observed little difference between control (no prepulse) and −80-mV prepulse test responses in a total of five experiments. These results appear to contrast with the findings of a contingent gating scheme for voltage-dependent gap junctions of amphibian blastomeres.

This work was supported by National Institutes of Health grants HL-42220 to R. D. Veenstra and HL-37702 to L. F. Lemanski.

Received for publication 24 April 1991 and in final form 24 February 1992.

REFERENCES

Beyer, E. C., D. L. Paul, and D. A. Goodenough. 1987. Connexin 43: a protein from rat heart homologous to a gap junction protein from liver. *J. Cell Biol.* 105:2621–2629.

Beyer, E. C., J. Kistler, D. L. Paul, and D. A. Goodenough. 1989. Antisera directed against connexin43 peptides react with a 43-kD protein localized to gap junctions in myocardium and other tissues. *J. Cell Biol.* 108:595–605.

Beyer, E. C., D. L. Paul, and D. A. Goodenough. 1990. Connexin family of gap junction proteins. *J. Membr. Biol.* 116:187–194.

Burt, J. M., and D. C. Spray. 1988. Single-channel events and gating behavior of the cardiac gap junction channel. *Proc. Natl. Acad. Sci. USA.* 85:3431–3434.

Ebihara, L., E. C. Beyer, K. I. Swenson, D. L. Paul, and D. A. Goodenough. 1989. Cloning and expression of a *Xenopus* embryonic gap junction protein. *Science (Wash. DC).* 243:1194–1195.

Eghbali, B., J. A. Kessler, and D. C. Spray. 1990. Expression of gap junction channels in communication-incompetent cells after stable transfection with cDNA encoding connexin32. *Proc. Natl. Acad. Sci. USA.* 87:1328–1331.

El Aoumari, A., C. Fromaget, E. Dupont, H. Reggio, P. Durbec, J.-P. Briand, K. Böller, B. Kreitman, and D. Gros. 1990. Conservation of a cytoplasmic carboxy-terminal domain of connexin43, a gap junction protein, in mammalian heart and brain. *J. Membr. Biol.* 115:229–240.

Fishman, G. I., D. C. Spray, and L. A. Leinwand. 1990. Molecular characterization and functional expression of the human cardiac gap junction channel. *J. Cell Biol.* 111:589–598.

Fishman, G. I., A. P. Moreno, D. C. Spray, and L. A. Leinwand. 1991. Functional analysis of human cardiac gap junction channel mutants. *Proc. Natl. Acad. Sci. USA.* 88:3525–3529.

Fox, J. A. 1987. Ion channel subconductance states. *J. Membr. Biol.* 97:1–8.

Giaume, C. 1991. Application of the patch clamp technique to the study of junctional conductance. *In* Biophysics of Gap Junction Channels. C. Peracchia, editor. CRC Press Inc., Boca Raton, FL. 175–190.

Harris, A. L., D. C. Spray, and M. V. L. Bennett. 1981. Kinetic properties of a voltage-dependent junctional conductance. *J. Gen. Physiol.* 77:95–117.

Jongsma, H. J., R. Wilders, A. C. G. van Ginneken, M. B. Rook. 1991. Modulatory effect of the transcellular electrical field on gap-junction conductance. *In* Biophysics of Gap Junction Channels. C. Peracchia, editor. CRC Press Inc., Boca Raton, FL. 163–172.

Laird, D. W., and J.-P. Revel. 1990. Biochemical and immunochemical analysis of the arrangement of connexin43 in rat heart gap junction membranes. *J. Cell Sci.* 97:109–117.

Lemanski, L. F., and Z. H. Tu. 1983. Immunofluorescent studies for myosin, actin, tropomyosin, and α-actinin in cultured cardiomyopathic hamster heart cells. *Dev. Biol.* 97:338–348.

Li, J., and L. F. Lemanski. 1990. Immunofluorescent studies for α-actinin in cultured cardiomyopathic hamster heart cells. *Anat. Rec.* 228:46–52.

Kameyama, M. 1983. Electrical coupling between ventricular paired cells isolated from guinea-pig heart. *J. Physiol. (Lond.).* 336:345–357.

Kanter, H. L., J. E. Saffitz, and E. C. Beyer. 1992. Cardiac myocytes express multiple gap junction proteins. *Circ. Res.* 70:438–444.

Makowski, L., D. L. D. Caspar, W. C. Phillips, and D. A. Goodenough. 1977. Gap junction structures. II. Analysis of the x-ray diffraction data. *J. Cell Biol.* 74:629–645.

Metzger, P., and R. Weingart. 1985. Electric current flow in cell pairs isolated from adult rat hearts. *J. Physiol. (Lond.).* 366:177–194.

Noma, A., and N. Tsuboi. 1987. Dependence of junctional conductance on proton, calcium, and magnesium ions in cardiac paired cells of guinea-pig. *J. Physiol. (Lond.).* 382:193–211.

Page, E., and C. K. Manjunath. 1986. Communicating junctions between cardiac cells. *In* The Heart and Cardiovascular System. Vol. II. H. A. Fozzard, E. Haber, R. B. Jennings, A. M. Katz, and H. E. Morgan, editors. Raven Press, New York. 573–600.

Rook, M. B., H. J. Jongsma, and A. C. G. van Ginneken. 1988. Properties of single gap junctional channels between isolated neonatal rat heart cells. *Am. J. Physiol.* 225(*Heart Circ. Physiol.* 24):H770–H782.

Rook, M. B., H. J. Jongsma, and B. de Jonge. 1989. Single channel currents of homo- and heterologous gap junctions between cardiac fibroblasts and myocytes. *Pfluegers Arch.* 414:95–98.

Rook, M. B., B. de Jonge, H. J. Jongsma, and M. A. Masson-Pévet. 1990. Gap junction formation and functional interaction between neonatal rat cardiocytes in culture: a correlative physiological and ultrastructural study. *J. Membr. Biol.* 118:179–192.

Rüdisüli, A., and R. Weingart. 1989. Electrical properties of gap junction channels in guinea-pig ventricular cell pairs revealed by exposure to heptanol. *Pfluegers Arch.* 415:12–21.

Spray, D. C., A. L. Harris, and M. V. L. Bennett. 1981. Equilibrium

properties of a voltage-dependent junctional conductance. *J. Gen. Physiol.* 77:77–93.

Swenson, K. I., J. R. Jordan, E. C. Beyer, and D. L. Paul. 1989. Formation of gap junctions by expression of connexins in *Xenopus* oocyte pairs. *Cell.* 57:145–155.

Veenstra, R. D. 1990. Voltage-dependent gating of gap junction channels in embryonic chick ventricular cell pairs. *Am. J. Physiol.* 258(*Cell Physiol.* 27):C662–C672.

Veenstra, R. D. 1991*a*. Developmental changes in regulation of embryonic chick heart gap junctions. *J. Membr. Biol.* 119:253–265.

Veenstra, R. D. 1991*b*. Comparative physiology of cardiac gap junction channels. *In:* Biophysics of Gap Junction Channels. C. Peracchia, editor. CRC Press Inc., Boca Raton, FL. 131–144.

Veenstra, R. D. 1991*c*. Physiological modulation of cardiac gap junction channels. *J. Cardiovasc. Electrophysiol.* 2:101–122.

Veenstra, R. D., and R. L. DeHaan. 1986. Measurement of single channel currents from cardiac gap junctions. *Science (Wash. DC).* 233:972–974.

Veenstra, R. D., and R. L. DeHaan. 1988. Cardiac gap junction channel activity in embryonic chick ventricle cells. *Am. J. Physiol.* 254(*Heart Circ. Physiol.* 23):H170–H180.

Veenstra, R. D., K. Berg, H.-Z. Wang, E. M. Westphale, and E. C. Beyer. 1992. Molecular and biophysical properties of the connexins from developing chick heart. *In* Gap Junctions. J. E. Hall and G. A. Zampighi, editors. Elsevier, Amsterdam. In press.

Wang, H.-Z., J. Li, L. F. Lemanski, and R. D. Veenstra. 1991. Properties of single gap junction channels between neonatal hamster cardiac myocytes. *Biophys. J.* 59:439*a*. (Abstr.)

Weingart, R. 1986. Electrical properties of the nexal membrane studied in rat ventricular cell pairs. *J. Physiol. (Lond.).* 370:267–284.

Werner, R., E. Levine, C. Rabadan-Diehl, and G. Dahl. 1989. Formation of hybrid cell-cell channels. *Proc. Natl. Acad. Sci. USA.* 86:5380–5384.

White, R. L., D. C. Spray, A. C. Campos de Carvalho, B. A. Wittenberg, and M. V. L. Bennett. 1985. Some electrical and pharmacological properties of gap junctions between adult ventricular myocytes. *Am. J. Physiol.* 249(*Cell Physiol.* 18):C447–C455.

Yancey, S. B., S. A. John, R. Lal, B. J. Austin, and J.-P. Revel. 1989. The 43-kD polypeptide of heart gap junctions: Immunolocalization, topology, and functional domains. *J. Cell Biol.* 108:2241–2254.

Zhang, J.-T., and B. J. Nicholson. 1989. Sequence and tissue distribution of a second protein of hepatic gap junctions, Cx26, as deduced from its cDNA. *J. Cell Biol.* 109:3391–3401.